Journal of Materials Chemistry A

PAPER

View Article Online
View Journal | View Issue

Cite this: J. Mater. Chem. A, 2019, 7, 12266

Boron nitride nanosheet embedded bio-inspired wet adhesives with switchable adhesion and oxidation resistance†

Biyu Jin,[a] Guangfa Zhang,[a] Jiazhang Lian,[b] Qinghua Zhang, *[ac] Xiaoli Zhan[ac] and Fengqiu Chen[a]

Smart adhesives that can debond from a surface on-command in response to stimuli are highly desired. However, the over-oxidation of mussel-mimetic adhesives greatly reduces free-catechol groups and results in an irreversible cross-linked network, especially in alkaline environments. Driven by the synergistic effects of reconstructive Schiff base equilibrium and adjustable dimethylaminoethyl methacrylate (DMAEMA) wettability, an insulated and bactericidal mussel-mimetic nanocomposite adhesive is developed with switchable adhesion and oxidation resistance. Amino-decorated boron nitride nanosheets serve as adhesive building blocks, which can interact with aldehyde group-terminated PEG side chains to form pH-responsive Schiff base networks *in situ*, reinforcing the cohesion of the adhesive. The alkaline-induced hydrophobic DMAEMA, displaying oxidation inhibiting effects, is subtly incorporated; it can maintain sufficient free-catechol groups to provide desirable adhesion and hinder the irreversible crosslinking of catechols. After acid treatment, the debonding of imine linkages together with acid-induced hydrophilic DMAEMA can drastically decrease bonding strength. Besides, the unique electric properties of BNNSs and the inherent antibacterial activity of Schiff bases endow the as-prepared adhesive with additional prominent functionality, such as high breakdown strength, a low dielectric constant, low dielectric loss and superior bactericidal effects against both Gram-positive and Gram-negative bacteria. This multifunctional adhesive may possess extensive applications in the biomedical and marine industries.

Received 15th March 2019
Accepted 5th April 2019

DOI: 10.1039/c9ta02827g

rsc.li/materials-a

1. Introduction

Smart adhesive materials with switchable adhesion properties are highly desired because they generate the great possibility of recycling these multicomponent materials.[1,2] Inspired by the strong adhesion capacity of DOPA-rich mussel plaque on various surfaces, considerable effort has been devoted to introducing stimuli-responsive components into catechol-containing adhesives.[3–5] For example, temperature-responsive *N*-isopropylacrylamide (NIPAM) allows the adhesion strength to be fully reversed below and above the LCST.[6] Photo-crosslinkable anthracene moieties contribute to a five-fold amplification of adhesion strength upon UV irradiation.[7] In addition, upon utilizing pH-responsive catechol-boronate coordination, successive contact cycle experiments demonstrate that as-prepared adhesives possess the ability to reversibly alter their interfacial work of adhesion from high to low upon changing the pH from 3 to 9.[8] However, high adhesion is usually desired in neutral or alkaline conditions in daily life or the marine industry, thus the acid-induced decline of adhesion forces is more desirable. In addition, advanced adhesives should demonstrate the conflicting properties of having both strong adhesion and stimuli-induced weakened binding strength.

As is commonly known, the strong adhesion of DOPA derivatives is generally attributed to the dual role of catechols. One aspect is that they provide interfacial adhesion through forming noncovalent interactions with adhered substrates, while the other aspect is that they enhance internal cohesion, mainly from quinone-mediated covalent crosslinking.[9–13] However, the 'Achilles' heel' of these materials is exactly due to catechols. Although catechol oxidation is propitious with regards to improving cohesion within bulk adhesives, the formed non-adhesive *o*-quinones are detrimental to interfacial adhesion.[14] It should be noted that the crosslinking of networks is generally irreversible, thus their repeated and multifunctional usage is considerably restricted, especially in basic environments where the auto-oxidation of catechols readily takes

[a]Zhejiang Provincial Key Laboratory of Advanced Chemical Engineering Manufacture Technology, College of Chemical and Biological Engineering, Zhejiang University, Hangzhou 310027, China

[b]Key Laboratory of Biomass Chemical Engineering, College of Chemical and Biological Engineering, Zhejiang University, Hangzhou 310027, China

[c]Institute of Zhejiang University-Quzhou, Quzhou 324000, China. E-mail: qhzhang@zju.edu.cn

† Electronic supplementary information (ESI) available. See DOI: 10.1039/c9ta02827g

place.[15–17] Unfortunately, the trade-off between strong and reversible adhesion with mussel-inspired adhesives is so far unsolved.

To restrict the irreversible crosslinking of catechols, some ingenious methods have been explored. For instance, through inserting dopamine into the confined nanospaces of clay nanosheets, a substantial degree of the oxidation of DOPA is prevented because of insufficient oxygen content.[15] Using protective groups, like borate or *tert*-butyldimethylsilyl chloride, to form bidentate catechol-boronate complexes or silylated catechol monomers also can protect phenolic hydroxyl groups and, as a consequence, eliminate oxidation fundamentally.[8,18] Another simple and efficient method is to introduce hydrophobic groups, including poly(styrene),[19] poly(*N*-isopropylacrylamide),[20] poly(methyl acrylate)[21] and the amyloid-based protein CsgA,[22] which can create a hydrophobic microenvironment or interact with aromatic side chains, thereby reducing the susceptibility of catechols to oxidation. On the basis of these points, we put forward that dimethylaminoethyl methacrylate (DMAEMA), displaying switchable hydrophobic and hydrophilic characteristics in response to pH adjustments, can potentially be used to intelligently stabilize and maintain a large amount of free-catechol on demand.

Here, we design a nanocomposite adhesive (NCA) with pH-induced switchable adhesion simply by mixing amino-functionalized boron nitride nanosheets (BNNSs) and a dopamine methacrylamide-DMAEMA-aldehyde group-modified PEG ternary copolymer. In neutral and alkaline environments, the as-prepared adhesive shows revocable outstanding bonding performance. First, sufficient free-catechol groups are reserved to physically attach onto substrates, contributed to by alkaline-induced hydrophobic protection from copious hydrophobic DMAEMA groups. Second, instead of utilizing the oxidation of catechol groups to crosslink the adhesive, aldehyde group-functionalized side chains allow another approach to enhancing cohesion. As assemblies of NCA building blocks, amino-decorated BNNSs can interact with the aldehyde groups to form pH-responsive imine linkages *in situ* at room temperature,[23] consequently maintaining the network integrity between the two disparate substrates. When the environment becomes acidic, the liquefaction of the adhesive drastically decreases the bonding strength, which is attributed to the debonding of imine linkages and acid-induced protonated hydrophilic DMAEMA (Scheme 1). Having such constructive characteristics, this BNNS crosslinked NCA possesses strong and reversible adhesion, from approximately 1.44 to 0.30 MPa, upon adjusting the pH from 9 to 3. Also, the unique electric properties of the BNNSs lead to the incorporation of additional functionality, such as high breakdown strength, a low dielectric constant and low dielectric loss, outperforming commercial insulation encapsulation adhesives. Moreover, benefitting from the inherent antibacterial activity of Schiff bases, the synthesized adhesive exhibits superior bactericidal effects against both Gram-positive and Gram-negative bacteria, with an antibacterial rate of more than 97%.

2. Experimental section

2.1 Materials

Ethanol was purchased from Sinopharm Chemical Reagent Co. The synthetic procedures related to *N*-(3,4-dihydroxyphenethyl) methacrylamide (DMA), aldehyde group-functionalized poly(ethylene glycol)methacrylate (FMPEG), amino functionalized *h*-BN (BN-NH_2) and the copolymer P(DMA-*r*-DMAEMA-*r*-FMPEG) (denoted as DDF) are presented in the ESI.†

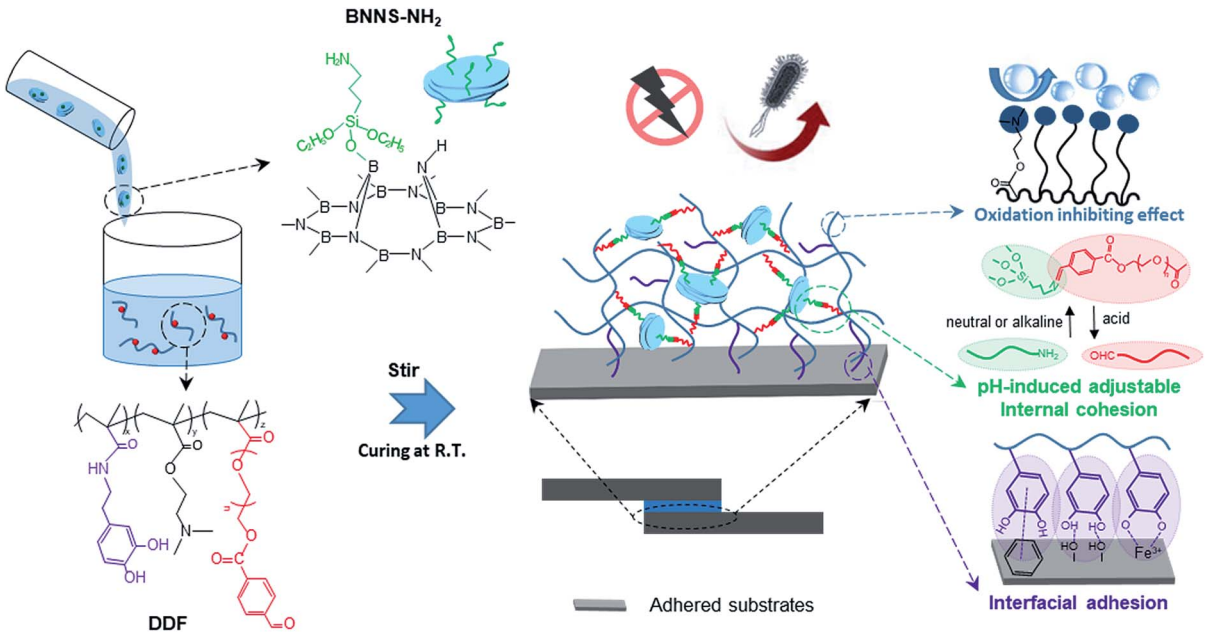

Scheme 1 The synthesis route of the NCA and its multiple characteristics (anti-bacterial, insulation, pH-induced switchable adhesion, and anti-oxidation).

2.2 Synthesis of the NCA (DDF-BNNS)

For P(DMA-*r*-DMAEMA-*r*-FMPEG)@BNNS-NH_2 gel preparation, DDF (1.2 g) in a mixture of 1 mL of water and 0.5 mL of ethanol is mixed with 100 μL of BNNS-NH_2 deionized water solution (60 mg mL^{-1}), followed by 10 min of room temperature stewing. For adhesion measurements, the obtaining of a crosslinked adhesive is not anticipated before coating onto slides, so we raise the amount of ethanol (1 : 1, v/v, ethanol/water) and lower the concentration (0.5 g mL^{-1}); thus the gelation process would occur on the test substrate slides after the evaporation of most of the ethanol during the 12 h stewing process. The detailed DDF-BNNS compositions are listed in Table 1.

2.3 Characterization

^{1}HNMR (Bruker Advance DMX500, 25 °C) and FT-IR (Nicolet 5700) characterization methods are used to analyze the chemical compositions of samples. A differential scanning calorimeter (DSC Q100) is used to examine the glass transition temperature (T_g) of DDF-BNNS samples with a ramp rate of 10 °C min^{-1}. The morphologies of exfoliated BNNSs and amino-modified BNNSs are observed under FESEM (Hitachi TM-1000) at an accelerating voltage of 20 kV. STEM images and energy dispersive X-ray spectroscopy (EDS) elemental maps are obtained using a Philips Tecnai G2 F20 S-TWIN electron microscope equipped with an Oxford X-MaxN detector at an acceleration voltage of 200 kV to confirm the existence and distribution of B, N, C, O and Si on the modified BNNSs. The elemental composition and chemical bonding properties of the adhesives are analyzed *via* X-ray photoelectron spectroscopy (XPS, Thermo Scientific, USA) with an Al Kα X-ray source. High-resolution spectra from the C1s and N1s regions are obtained.

The obtained samples are used for contact angle (WCA) measurements, which are performed using a CAM 200 optical contact-angle goniometer (KSV Co., Ltd., Helsinki, Finland) at room temperature to calculate the surface work of adhesion (W_{SA}; more details in the ESI†). Mechanical properties are obtained and lap shear tests are conducted using a Zwick/Roell Z020 universal material tester. Typically, a sample is clamped at one end and pulled at a constant rate (100 mm min^{-1}) of elongation from the other clamped end using different fixtures. All tests are performed at room temperature (more details in the ESI†). Rheological measurements are performed using an ARES-G2 rheometer. For strain sweeps (0.01 to 100%), the temperature and angular frequency are 30 °C and 6.28 rad s^{-1}, respectively. For frequency sweeps (0.1 to 100 rad s^{-1}), the temperature and strain are 30 °C and 0.5%, respectively. Dielectric breakdown strength measurements are performed with a homemade device using an electrostatic pull-down method under a DC voltage ramp of 1 V s^{-1} (more details in the ESI†). The plate count method is applied to investigate the effects of the resultant adhesives against *C. glutamicum* and *E. coli* (more details in the ESI†). pH-induced switchable adhesion tests are conducted by circularly adding 0.1 M HCl solution (to pH 3) and 0.1 M $NH_3 \cdot H_2O$ solution (to pH 9) into DDF solution (0.5 g mL^{-1}, 1 : 1 v/v ethanol/water), and taking 100 μL of the solution periodically onto the surface of PS, using a pipette, to conduct lap shear tests. UV-vis absorption spectra over a range from 250 to 600 nm are collected using a SHIMADZU UV-2550 spectrometer.

Table 1 Compositions of the DDF-BNNS nanocomposites

Sample	DMA/DMAEMA/FMPEG[a]	BNNS[b]	DMA content (wt%)
DDF 1	5/80/15	0	5
DDF 2	10/80/10	0	10
DDF 3	15/80/5	0	15
DDF-BNNS1	10/80/10	1	10
DDF-BNNS2.5	10/80/10	2.5	10
DDF-BNNS5	10/80/10	5	10
DDF-BNNS7	10/80/10	7	10
DDF-BNNS10	10/80/10	10	10

[a] Mole ratio. [b] Mass ratio, m(BNNS) : m(DDF).

3. Results and discussion

3.1 Preparation of the NCA

h-BN is initially exfoliated in DMF solution and then modified with KH550 *via* the hydrolytic condensation of triethoxysilane, giving rise to the appearance of many reactive amino groups at the same time (BNNS-NH_2, Scheme S1†). The ultrasonic exfoliating process can produce ultra-thin BNNSs (thickness of about 3 nm) without damage to the lattice integrity (Fig. S3†).[24] The appearance of O, C and Si speaks in the XPS spectrum of BNNS-NH_2 confirms the successful modification (Fig. 1d). Infrared absorption peaks at 858 cm^{-1} and from 2974 to 2887 cm^{-1} and the broad band from 3650 to 3200 cm^{-1} are assigned to Si–O, alkyl groups and N–H from KH550, respectively (Fig. 1c). The graft density is calculated to be about 0.2 grafted amino groups per nm^2, according to EDS analysis (Fig. S4†) and previous work.[25]

In the subsequent process, BNNS-NH_2 is mixed with catechol-rich copolymers (DDF, Scheme 1) and cured at a mild temperature within a few minutes (Scheme S1e†). Thanks to the satisfying hydrophilic nature of the terminated amino groups, achieving a homogeneous dispersion of BNNSs in the adhesive network becomes much easier, even at a high BNNS feeding ratio, which is of great importance to the overall cohesiveness of DDF-BNNS. As revealed by cross-sectional SEM images and TEM images (Fig. 1a–b and S5†), amino-functionalized BNNSs are loosely distributed in the copolymer without apparent agglomeration with a 10 wt% content. EDS mapping of the B, N and Si elements in DDF-BNNS10 (Fig. 1b) further confirm this.

As seen in the FT-IR spectra in Fig. 1c, the peaks at 1629 cm^{-1} and 1525 cm^{-1} correspond to the stretching vibrations of –CONH– bending deformation, and the broad band from 3100–3600 cm^{-1} can be ascribed to N–H and –OH groups from DMA that remain after polymerization. The absorption band at 1350 cm^{-1} can be ascribed to C–N stretching vibrations, indicating the existence of DMAEMA in the spectra of DDF-BNNS. Upon performing crosslinking with the copolymer DDF by enhancing the mass ratio of the crosslinker BNNS-NH_2 from 1.0 to 10.0 in the feed, a sharp peak emerges at 1672 cm^{-1},

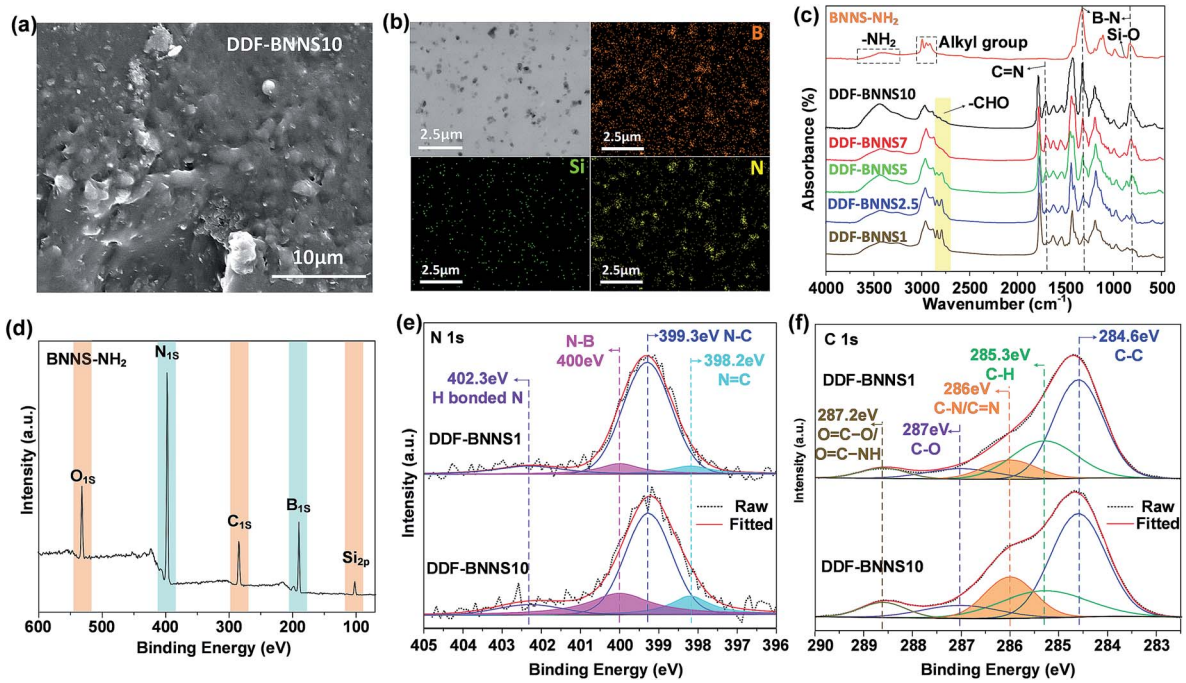

Fig. 1 (a) SEM and (b) TEM images and element mapping of DDF-BNNS10; (c) FTIR spectra of BNNS-NH_2 and DDF-BNNS samples with different BNNS-NH_2 content values; (d) the XPS spectrum of BNNS-NH_2; and (e) N 1s core-level and (f) C 1s core-level spectra of DDF-BNNS1 and DDF-BNNS10.

corresponding to imine groups, and the intensity gradually increases; this is accompanied by the fading of the absorption peaks from aldehyde groups (peaks at 2822 cm^{-1} and 2772 cm^{-1}), confirming the formation of a chemically crosslinked network. Meanwhile, visible increases in the absorption intensities at 1274 cm^{-1} and 807 cm^{-1} associated with B–N are observed.

These results are further verified by XPS, as shown in Fig. 1e–f. The N 1s peak can be deconvoluted into four peaks corresponding to N=C binding at 398.2 eV, N–C bonding at 399.3 eV, N–B imine bonding at 400 eV, and H-bonded N at 402.3 eV.[26,27] In the C 1s spectrum, the fitted peaks located at 284.6, 285.3, 286.0, 287.0 and 288.6 eV are assigned to C–C, C–H, C=N/C–N, C–O and O=C–O/O=C–NH species, respectively.[26] With increasing BNNS content, the intensities of the N=C, N–B, and C=N/C–N peaks increase significantly (Fig S6, Tables S1 and S2†). This implies that amino groups located on BNNS are taking part in condensation reactions with aldehyde groups hanging on the copolymer chains to form a crosslinked Schiff base network. This is consistent with the results from DSC experiments (Fig. S7†). For example, prior to crosslinking, DDF has a glass transition temperature (T_g) of −15.70 °C. After crosslinking with 10% BNNS-NH_2 to form DDF-BNNS10, T_g increases to 20.22 °C, as would be expected due to the effects of crosslinking and tough nanosheets.

3.2 Strong and switchable adhesion properties

Three copolymer samples are synthesized with different mole ratios of *N*-(3,4-dihydroxyphenethyl)methacrylamide, 2-(dimethylamino)ethyl methacrylate and aldehyde group-functionalized poly(ethylene glycol)methacrylate. As displayed in Fig. 2a, the lyophilized product is a light-yellow powder without stickiness. After being immersed in a few water droplets, the powder becomes a highly sticky and water-insoluble coacervate. To further research the effects of water content on the adhesion performance, DDF2 samples with different water content levels were tested (Fig. 2a4). With a decrease in the water content from 118.1% to 30.4%, the shear stress increases 10 times, from 0.11 MPa to 1.09 MPa, as higher solid fractions lead to more sufficient interactions between the adhesive and glass. However, a severe decrease in the water content to 7.1% resulted in brittle interfacial adhesion, which relates to a certain water content. The bonding strengths of linear adhesives with different catechol compositions are quantified through lap shear testing using representative surfaces with different surface energies (Fig. 2g). For stainless steel (SS) and polystyrene (PS), DDF3, with the highest mole content of the DMA monomer, displays the highest adhesion strength. This can be explained by the fact that having a greater number of catechol groups is not only beneficial for coordinating with Fe^{3+} *via* phenolic hydroxyl groups in relation to SS,[28] but it is also positive for forming aromatic interactions with benzene rings of PS.[29] For glass, aluminum (Al) and polytetrafluoroethylene (PTFE), the optimum adhesion performance appears when the molar ratio of DMA, DMAEMA and FMPEG is 10 : 80 : 10. This is understandable, since both the suitable wettability and special interactions in relation to DMA make positive contributions to bulk adhesion. More hydrophilic adhesives are believed to exhibit greater interfacial interactions with immersed substrates; this is utilized for adhesive action.[30] The smaller water contact angles in air associated with the larger surface

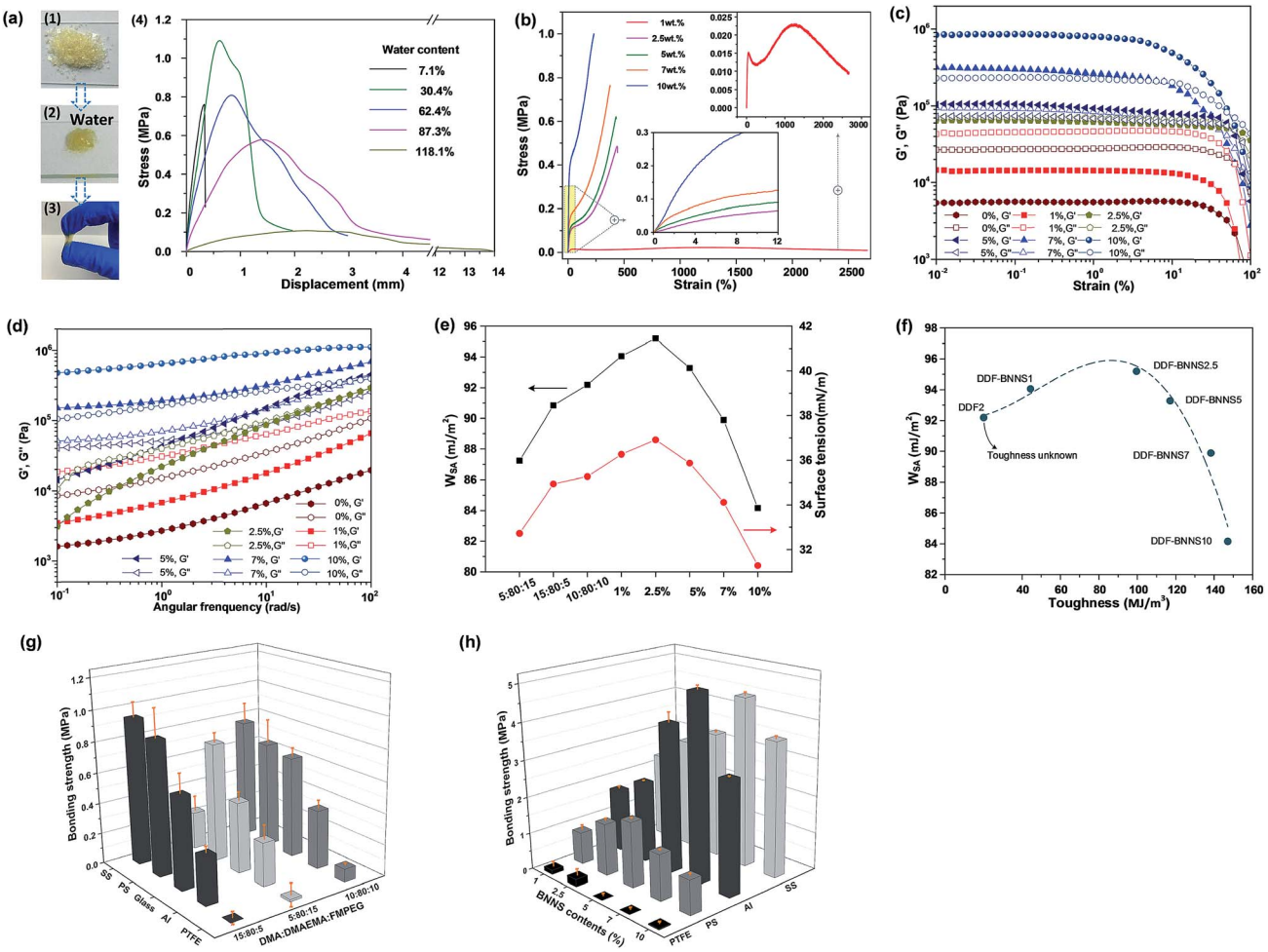

Fig. 2 (a) Photos of DDF2 before (1) and after (2) immersion in water, and (3) sticking to a nitrile glove; and (4) tensile–strain curves of glass slide samples bonding with DDF2 with variable water content levels. (b) Stress–strain curves of DDF-BNNS samples with different BNNS-NH_2 content. Storage (G') and loss modulus (G'') values of DDF2, DDF-BNNS1, DDF-BNNS2.5, DDF-BNNS5, DDF-BNNS7 and DDF-BNNS10 following (c) strain and (d) frequency sweeps. (e) The surface work of adhesion and surface tension of DDF-BNNS samples as a function of BNNS-NH_2 addition. (f) Surface work of adhesion values as a function of toughness. (g) Bonding strength values as a function of various materials and the molar ratios of DMA, DMAEMA and FMPEG. (h) Bonding strength values as a function of various materials and the mass addition of BNNS-NH_2.

work of adhesion (W_{SA}) values of DDF2 and 3 (Fig. 2e and Table S3†) are shown to provide further proof.

Notably, the adhesion performances of synthetic linear mussel-mimetic adhesives (DDF series) are inferior to some similar reported adhesives.[31] From UV-vis spectra of DDF2, the presence of only one characteristic peak at 283 nm reveals a mass of catechol groups after dissolution in a mixture of neutral water and ethanol solution for 12 h (Fig. 3f). This means that bulk adhesion of linear DDF mainly results from interfacial interactions and a small number of weak internal interactions from catechol side chains because the oxidation crosslinking process was greatly hampered by the presence of a large proportion of hydrophobic DMAEMA. This anti-oxidation characteristic is extremely crucial to reversibly switch the adhesion properties of the prepared adhesives over a wide pH range, which will be discussed later.

In order to obtain high bonding strength, but not at the expense of fractional interfacial adhesion, and enable switchable adhesion at the same time, we carried out a BNNS cross-linking process to the linear adhesives. The imine linkages between BNNSs and copolymer chains can uncouple and recouple dynamically upon the addition of acid and alkaline solutions, thereby imparting adhesion adjustability. A series of adhesives with different weight ratios of BNNS-NH_2 to DDF2 are fabricated. The highest bonding strengths to PTFE, PS, Al and SS can reach as much as 0.42 MPa, 1.97 MPa, 5.20 MPa and 4.75 MPa, respectively, which are 1.79, 2.37, 9.88 and 5.17 times higher than the corresponding values for DDF2. As the W_{SA} values of DDF2 and DDF-BNNSs range on average from 89.89 to 95.20 mJ m^{-2}, the main difference lies in whether or not BNNS-NH_2 was incorporated, which clearly testifies to the function of BNNS-NH_2 as a chemical cross-linker. Notably, due to the brittle nature of glass, bonding strength data for crosslinked adhesives on this surface are unavailable on account of the prior rupturing of glass, as demonstrated in Video S1.† A qualitative weight-loading test indicated that a DDF-BNNS2.5 merged glass lap joint could readily support a heavy load of 1.67 kg (Fig. S8†).

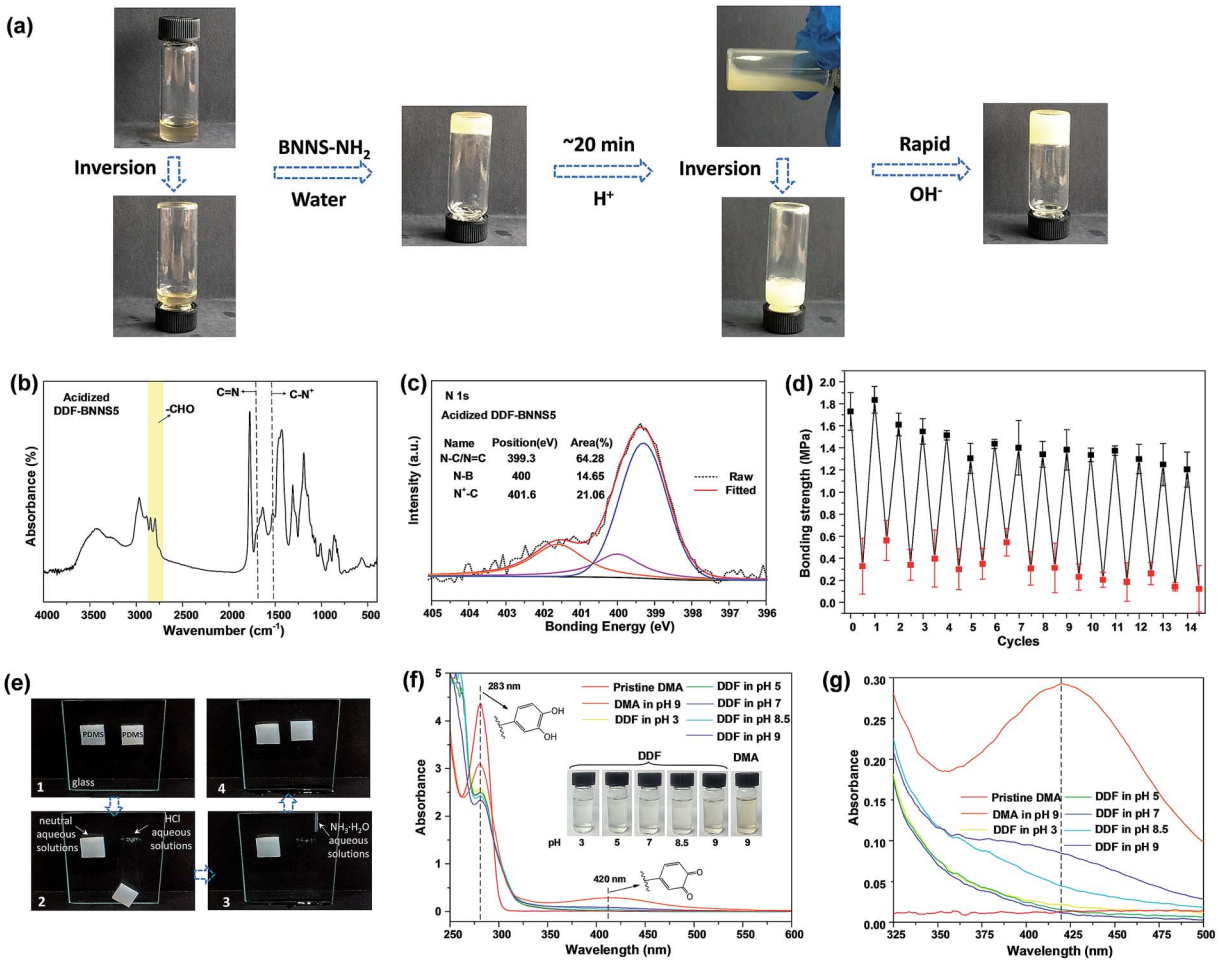

Fig. 3 (a) The dynamic bonding and debonding processes of DDF-BNNS2.5. (b) FTIR and (c) XPS spectra of acidified DDF-BNNS5. (d) Switching the adhesion properties *via* circularly controlling pH from 9 to 3 to 9 (PS, DDF-BNNS5). (e) The selective pH-induced release of PDMS from glass. (f) UV-vis spectra of DMA and DDF in solutions with different pH values; the inset shows photos after diluting six time for UV-vis tests. (g) An enlargement of (f) from 325 to 500 nm.

We discover that bonding strengths of DDF-BNNS adhesives are generally affected by the surface energies of the applied substrates and the BNNS content. As the surface energy increases in the following sequence: PTFE (~20 mN m^{-1}) < PS (36.97 mN m^{-1}) < Al (155 mN m^{-1}) < SS (241 mN m^{-1}),[32] so does the optimal dosage of BNNS-NH_2, from 2.5% to 5% to 7% (Fig. 2h and Table S6†). Increasing the BNNS-NH_2 content does not result in a linear increase in the bulk bonding strength because the bulk bonding strength is a synergistic outcome of interfacial adhesion and internal cohesion.[30] First of all, more BNNSs featuring more reactive amino groups can have a favorable effect on accelerating the crosslinking degree of linear adhesives and, as a consequence, increasing internal cohesion (Fig. 2b and Table S4†). The Young's modulus and toughness of DDF-BNNS10 increase 71.12 times and 2.31 times, respectively, compared with DDF-BNNS1. However, worse interfacial adhesion is actually an outcome of excessive BNNS-NH_2 content. An increase in internal cohesion is accompanied by a sharp drop in interfacial adhesion after the peak value (Fig. 2f). In other words, a tighter cross-linked network attenuated the adhesive hydrophilicity (Table S5†) and restrained the contact of polymer chains with substrates at the adhesion interface. Rheological measurements are performed to probe the structural property changes in bulk samples. In Fig. 2c, the G' and G'' values of DDF-BNNS samples increase more than an order of magnitude upon increasing BNNS-NH_2 addition, which is attributed to a stiffer network and growing T_g values. As the strain increases, both the G' and G'' values of DDF-BNNS samples undergo a downward trend because of polymer chain disentanglements at higher shear strain values and a crossover of these is observed for DDF-BNNS10, DDF-BNNS7, DDF-BNNS5 and DDF-BNNS2.5 when the strain is more than 10%. These samples transform from having elastic character to having fluid character above the critical strain. However, DDF2 and DDF-BNNS1 present dominant viscous behavior with $G'' > G'$ over the entire strain range. Fig. 2d shows the dynamic frequency sweep spectra of bulk samples in the linear viscoelasticity region. Within the measured frequency range, all G' and G'' values increase with increasing frequency; this may be because of DDF-BNNS, with its soft flexible FMPEG side chains, allowing recovery from

Table 2 A comparison of performance between different adhesives

Adhesive	Curing time	Tuning tool	Adjustable adhesion	Maximum bonding strength (MPa)	Ref.
P(DMA-*r*-DMAEMA-*r*-FMPEG) @BNNS-NH_2 (DDF-BNNS)	12 h, R.T.	pH (3 and 9)	1.44 to 0.30 MPa from pH 9 to 3 (PS, reversible)	> 0.8 (glass) 0.42 (PTFE, DDF-BNNS2.5, pH 7) 1.97 (PS, DDF-BNNS5, pH 7) 5.20 (Al, DDF-BNNS7, pH 7) 4.75 (SS, DDF-BNNS7, pH 7)	This work
P(MDOPA-*co*-SBMA-*co*-NBDM)	24 h, R.T.	UV light irradiation (352 nm)	341 to 150 kPa (mylar film, irreversible)	0.341 (mylar film)	33
P(benzyl ether)	24 h, R.T.	Fluoride solution TBAF	0.51 to 0.05 MPa by adding 0.1 M TBAF (glass, irreversible)	0.51 (glass)	34
PAMAM-*g*-diazirine	0–10 min, R.T.	Low-voltage activation (−2 V)	Tunable around *ca.* 0.01–0.08 MPa (ITO, irreversible)	*ca.* 0.08 (ITO glass) *ca.* 0.025 (PET) *ca.* 0.02 (glass)	35
1,4-Butanediol-poly[(EG2-Glu)-co-(DOPA)] (BPED); BPEDA; BPEDAC; BPEDAL	0–25 h	Functional polypeptide side groups; temperature	25 °C and 37 °C: *ca.* 46 and 60 kPa for BPED; *ca.* 56 and 76 kPa for BPEDA; *ca.* 80 and 85 kPa for BPEDAC; *ca.* 88 and 101.2 kPa for BPEDAC- BPEDAL (porcine skin, irreversible)	0.1012 (porcine skin, BPEDAC-BPEDAL, 24 h) 0.603 (bone, BPEDAC-BPEDAL, 24 h)	36
P(DOPA-*co*-AD-*co*-MEA)-P(NIPAM-*co*-CD)	None	Temperature	*ca.* 3 to 0.25 kPa from 40 °C to 25 °C (glass, Si, Ti, Al, PTFE, reversible)	*ca.* 0.01 (rough PDMS pillar arrays, 40 °C)	6
Cucurbit[*n*]uril supramolecular	50 °C for 3 min	None	None	*ca.* 1.5 (glass, Al, SS) *ca.* 1 (Cu) *ca.* 2.25 (bone) *ca.* 9 (wood)	37

deformation in different frequency regions. DDF-BNNS5 and DDF-BNNS2.5 display crossover between G'' and G', whereas DDF-BNNS10 and DDF-BNNS7 display solid-like behavior with G' higher than G'' over the entire frequency range, revealing an enhanced degree of crosslinking in the elastomeric network. For materials with low surface energy (PTFE), sufficient interfacial adhesion, such as in the case of DDF-BNNS2.5 with the highest W_{SA} value (Fig. 2e), in theory is necessary to avoid "interface fracture", which is in accordance with the observed values. For high surface energy materials (Al and SS), there is a tendency to reduce the asymmetrical forces of solid surface molecules, thereby reducing the surface tension and surface Gibbs free energy and making it easier to stick to adhesives, resulting in a "bulk fracture" dominated fracture mode. In this case, an appropriate amount of BNNSs, such as 7 wt%, could guarantee strong cohesion and simultaneously ensure that interfacial adhesion is optimal.

Different pH environments can reform the equilibrium of Schiff bases, thus leading to the dissolution and crosslinking of the NCA (Fig. 3a, Video S2–S4†). The prepared NCA exhibits tunable adhesion forces in response to acid and alkaline solutions. For example, the bonding strength of PS slides is measured to be 1.73 MPa with a DDF-BNNS5 joint. Acidifying the adhesive with 0.1 M HCl solution (to pH 3) could result in the deactivation of internal cohesion, giving a low bonding strength of 0.33 MPa. The acid-induced debonding process can be inferred from the disappearance of the peak from imine groups (1672 cm^{-1}) together with the increased intensities of the aldehyde group peaks (2822 cm^{-1} and 2772 cm^{-1}) in FTIR spectra (Fig. 3b). Notably, this value is much lower than DDF2 (0.83 MPa), which could be the result of protonated DMAEMA side chains. When the pH decreases below the pK_a value (7.2) of tertiary amine groups, the presence of too many cationic charges proves to be detrimental to adhesion performance because of electrostatic repulsion interactions.[18] After acid treatment, the C–N peak shifts from 1350 cm^{-1} to 1493 cm^{-1} in the FTIR spectra, which is ascribed to $C–N^+$ (Fig. 3b). In addition, the area of the $C–N^+$ quaternary ammonium bond peak at 401.6 eV is estimated to be 21.06% (Fig. 3c). Re-treating the acidified adhesive with 0.1 M $NH_3 \cdot H_2O$ solution (to pH 9) again brings about a recovery of the bonding strength, displaying a fully reversible signature. However, a decaying trend in adhesion strength is observed over continuous 14 cycles (Fig. 3d). As the neutralization reaction between hydrochloric acid and ammonium hydroxide generates salt residues in the adhesive, embrittlement as a result of this gives rise to the likelihood of "bulk fracture". The increasing storage modulus and decreasing breakage elongation of DDF-BNNS5 from 2.01 to 3.98 MPa and from 429.55% to 224.75%, respectively, after 14 cycles confirm the generation of an increasingly hard and brittle adhesive, which is not suited to energy dissipation (Fig. S13a†). DSC results from DDF-BNNS5 show a growing T_g value from

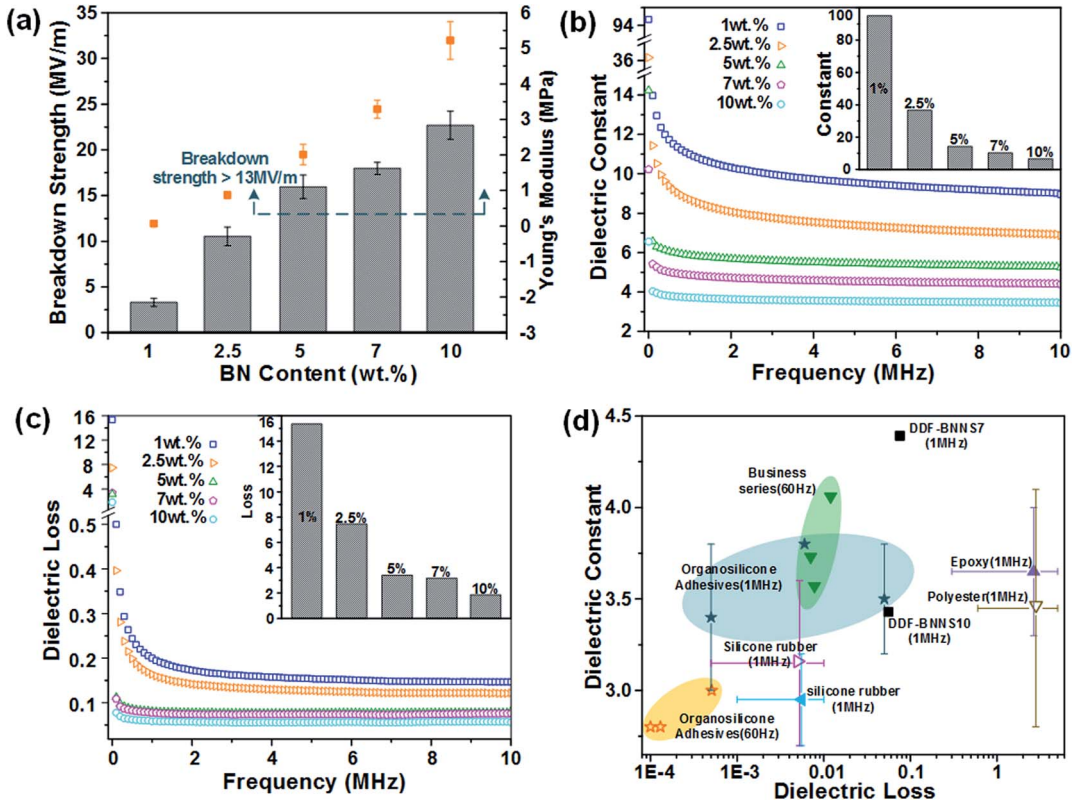

Fig. 4 (a) The breakdown strength of DDF-BNNS with different BNNS-NH_2 content. The frequency-dependent dielectric constant (b) and loss (c) of DDF-BNNS with different BNNS-NH_2 content; inset: dielectric constant (b) and loss (c) of DDF-BNNS with different BNNS-NH_2 content at 20 MHz. (d) A comparison of dielectric constant and loss values between different adhesives and insulating materials.

5.70 °C to 16.98 °C after 14 cycles, providing further evidence (Fig. S13b†). Regardless of this, adhesion strength still can be adjusted by over an order of magnitude during long cycling.

Hydrophobic pDMAEMA is considered to guarantee switchable adhesion because effective anti-oxidation effects inhibit irreversible catechol-functionalized copolymer cross-linking. DMA and DDF are dispersed in an ethanol-water mixture (1 : 1 v/v, 0.5 g mL^{-1}) for 12 h and analyzed *via* UV-visible spectroscopy. As demonstrated in Fig. 3f and g, the absorption band in the region of 350–500 nm^{-1} is attributed to dopaquinone, indicating the occurrence of an oxidation process. Compared to DMA at pH 9, the absorption peaks from DDF at pH 9 and pH 8.5 decrease sharply, while being barely perceptible at pH 3, 5 and 7, revealing a mild or negligible oxidation process. Digital images (inset of Fig. 3f) show the visible coloration of the DDF solution as the pH is raised, due to generated polydopamine.

To visually illustrate the rapid pH-regulated bonding and debonding process of the NCA, two polydimethylsiloxane squares (weight: 2.7 g; 20 mm × 23 mm × 5 mm) are glued to vertically standing glass using DDF-BNNS7 at the upper edges. As illustrated in Fig. 3e, both squares can support their own weight without flopping at the beginning. After this, an identical volume of neutral or acid aqueous solution is added to the interface between the PDMS square and the glass at the upper edge. There was no macroscopic influence on the left PDMS square and it remained motionless, in stark contrast to the right one. After being treated with 0.1 M HCl solution, the prompt falling of the PDMS square from the glass within just 1 min was observed. Interestingly, the dismissed adhesion is recoverable after treatment with 0.1 M $NH_3 \cdot H_2O$ solution. Following the wiping off of superfluous solution, the reunited coacervates regained adhesion to the PDMS square. This switchable adhesion behavior endows DDF-BNNS with the ability to serve as an efficient and selective pH-responsive adhesive. Movie S5† depicts the pH-responsive process.

We also make a comparison with some state-of-the-art adhesives to comprehensively evaluate the adhesion performance of DDF-BNNS in Table 2. It is clearly observed that DDF-BNNS exhibits prominent bonding strength onto materials with different surface energies, as well as a wide switchable adhesion force range, outperforming most other responsive adhesives.

3.3 Dielectric and antibacterial properties

The wide band gap and high plane hardness of BNNS homodispersed in a copolymer matrix play the role of providing an efficient barrier against electrical conduction and endow the BNNS-embedded adhesives with higher breakdown strength, a lower dielectric constant and lower dielectric loss relative to the pure copolymer, which suitably positions the adhesive as an insulation paste for electrical equipment.[38] Fig. 4a presents the variations in breakdown strength upon varying the BNNS content; with an increase in the addition amount from 1% to

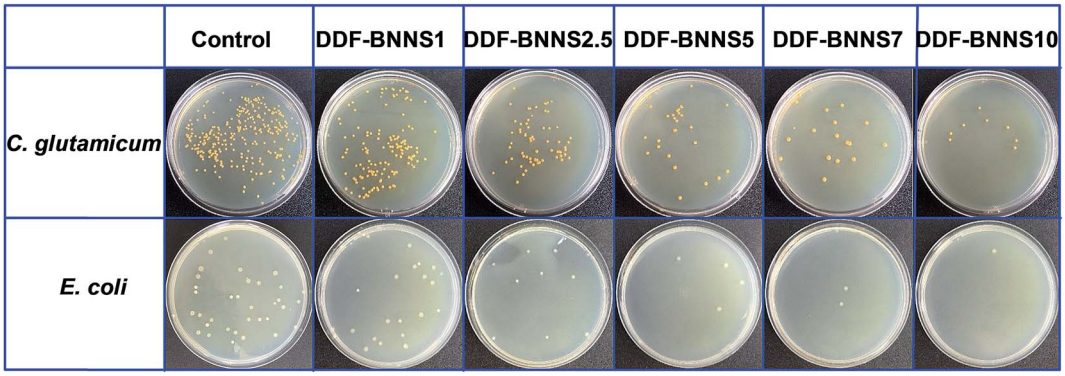

Fig. 5 Antibacterial activities against Gram-positive and Gram-negative bacteria after 2 h of contact time on glass coated with different samples.

10%, the breakdown strength greatly increased from 3.31 to 22.71 MV m^{-1}, which is comparable to most commercial adhesives (13 to 25 MV m^{-1}) and even several insulating materials, such as RTV-1 and RTV-2 silicone rubber (20 to 30 MV m^{-1}), epoxy (21 to 50 MV m^{-1}) and polyester (15 to 38 MV m^{-1}). Basically, the BNNSs play a dual role in improving the electric breakdown strength of DDF-BNNS. On the one hand, with an increase in BNNS content, the resistivity becomes much higher due to more insulated nanofillers. On the other hand, a higher Young's modulus and better mechanical properties are achieved, which are conducive in acting as a robust barrier to resist electromechanical failure. Moreover, the dielectric constant and dielectric loss tangent of insulation encapsulation adhesives used in electrical engineering should be satisfied at a low level. The dielectric constant representing the accumulation of electrostatic energy per volume per unit of electric field is desired to be small. In order to reduce the negative influence on the network from self-heating phenomena, a low dielectric loss is necessary, especially under high frequency where the power loss is proportionally increased. As seen in Fig. 4b and c, an increased dosage of BNNSs generates a pronounced reduction in the dielectric constant and dielectric loss, *e.g.*, from 8.94 and 0.147 for DDF-BNNS1 to 3.43 and 0.056 for DDF-BNNS10, respectively, at 1 MHz. Meanwhile, both are kept stable at low values over a wide range of high frequencies from 1 to 10 MHz, *e.g.*, a dielectric constant between 3.33 and 3.46 and a dielectric loss between 0.055 and 0.059 are achieved for DDF-BNNS10, which are comparable to commercial insulation encapsulation adhesives, as shown in Fig. 4d.[39]

Schiff base (especially aromatic Schiff base) groups featuring C═N double bonds possess antibacterial and antitumor biological activities through scavenging overproduced reactive oxygen species (ROS) and coordinating with metal ions in cells to form stable compounds through lone pair electrons from N hybridization orbitals of imine groups.[40] The antibacterial properties of the NCA are investigated through the growth of Gram-positive *C. glutamicum* and Gram-negative *E. coli* in LB agar plates using a plate count method. As summarized in Fig. 5 and Table 3, visible gradient differences in colony numbers could be observed as the BNNS content varies. The sterilizing rate of DDF-BNNS1 was 37.07% for *C. glutamicum* and 26.47% for *E. coli*, while the corresponding values rose by up to more than 97% for both bacteria at the maximum C═N% for DDF-BNNS10. According to the standard reduction of bacteria criteria, over 70% reduction is considered to be a powerful bactericidal effect.[41] These results demonstrate that our NCA possesses superior antibacterial performance, thus hinting at a promising pathway for application in biomedical and related fields.

Table 3 Antibacterial efficiency of DDF-BNNS (% inhibition)

Sample	*E. coli*	*C. glutamicum*
Control	0	0
DDF-BNNS1	26.47%	37.07%
DDF-BNNS2.5	70.59%	74.90%
DDF-BNNS5	82.35%	88.80%
DDF-BNNS7	91.18%	94.14%
DDF-BNNS10	97.06%	98.05%

4. Conclusions

In summary, we demonstrate a nanocomposite adhesive with pH-induced switchable adhesion capabilities (reversed between 0.30 and 1.44 MPa) due to dynamic imine linkage equilibrium driven by different pH environments. Shielded by hydrophobic DMAEMA, the adhesive displays an oxidation inhibiting effect that can maintain sufficient amounts of free-catechol groups, even in alkaline solution (pH 9) for 12 h, which is responsible for the durable interfacial adhesion. The uniformly dispersed boron nitride nanosheets act as covalent cross-linkers and can greatly reinforce the cohesion of the adhesive. Consequently, the bulk bonding strength, controlled by the substrate surface energy, interfacial adhesion and internal cohesion, significantly achieved efficient enhancement compared with previously reported stimuli-responsive adhesives. Moreover, BNNSs with a wide band gap and high plane hardness impart the as-prepared adhesives with high breakdown strength (22.71 MV m^{-1}), a low dielectric constant and low dielectric loss (3.43 and 0.056, respectively, for DDF-BNNS10 at 1 MHz). Additionally, benefiting from the intrinsic antibacterial activity of Schiff bases, the synthesized adhesives show superior bactericidal effects against Gram-positive and Gram-negative bacteria (more than 97% for DDF-BNNS10). Therefore, the multifunctional adhesive shows extensive application prospects for the

biomedical and marine industries or other related fields. Note that we can replace BNNSs with other amino-functionalized nanofillers, such as CNTs, Fe_3O_4, Ag, *etc.* The adhesives can be infused with properties as desired, for example conductivity, magnetism, enhanced bactericidal activity, *etc.* We believe that the unique NCA structure is useful for further fundamental research and broad applications.

Conflicts of interest

There are no conflicts to declare.

Acknowledgements

The authors gratefully acknowledge the financial support provided by the National Natural Science Foundation of China (No. 21476195, 21576236 and 21676248) and the Zhejiang Provincial Major Project of Science & Technology for Award No. 2014C13SAA10006.

References

1 Y. Wang, H. Tian, J. Shao, D. Sameoto, X. Li, L. Wang, H. Hu, Y. Ding and B. Lu, *ACS Appl. Mater. Interfaces*, 2016, **8**, 10029–10037.
2 S. Baik, D. W. Kim, Y. Park, T. Lee, S. H. Bhang and C. Pang, *Nature*, 2017, **546**, 396–400.
3 J. H. Waite, *J. Exp. Biol.*, 2017, **220**, 517–530.
4 N. Chen, L. Qin and Q. Pan, *J. Mater. Chem. A*, 2018, **6**, 6667–6674.
5 H. Yang, C. Ma, K. Li, K. Liu, M. Loznik, R. Teeuwen, J. C. M. V. Hest, X. Zhou, A. Herrmann and J. Wang, *Adv. Mater.*, 2016, **28**, 5008–5012.
6 Y. Zhao, Y. Wu, L. Wang, M. Zhang, X. Chen, M. Liu, J. Fan, J. Liu, F. Zhou and Z. Wang, *Nat. Commun.*, 2017, **8**, 2218.
7 T. Harper, R. Slegeris, I. Pramudya and H. Chung, *ACS Appl. Mater. Interfaces*, 2017, **9**, 1830–1839.
8 A. R. Narkar, B. Barker, M. Clisch, J. Jiang and B. P. Lee, *Chem. Mater.*, 2016, **28**, 5432–5439.
9 P. K. Forooshani and B. P. Lee, *J. Polym. Sci., Part A: Polym. Chem.*, 2017, **55**, 9–33.
10 Y. Jeong, Y. K. Jo, B. J. Kim, B. Yang, K. I. Joo and H. J. Cha, *ACS Nano*, 2018, **12**, 8909–8919.
11 M. A. Gebbie, W. Wei, A. M. Schrader, T. R. Cristiani, H. A. Dobbs, M. Idso, B. F. Chmelka, J. H. Waite and J. N. Israelachvili, *Nat. Chem.*, 2017, **9**, 473–479.
12 L. Chen and Z. Guo, *Colloids Surf., A*, 2018, **554**, 253–260.
13 C. Gao, G. Li, H. Xue, W. Yang, F. Zhang and S. Jiang, *Biomaterials*, 2010, **31**, 1486–1492.
14 W. Wei, J. Yu, C. Broomell, J. N. Israelachvili and J. H. Waite, *J. Am. Chem. Soc.*, 2012, **135**, 377–383.
15 L. Han, X. Lu, K. Liu, K. Wang, L. Fang, L. Weng, H. Zhang, Y. Tang, F. Ren, C. Zhao, G. Sun, R. Liang and Z. Li, *ACS Nano*, 2017, **11**, 2561–2574.
16 B. P. Lee, P. B. Messersmith, J. N. Israelachvili and J. H. Waite, *Annu. Rev. Mater. Res.*, 2011, **41**, 99–132.
17 J. Yang, S. M. Cohen and M. Kamperman, *Chem. Soc. Rev.*, 2014, **43**, 8271–8298.
18 J. D. White and J. J. Wilker, *Macromolecules*, 2011, **44**, 5085–5088.
19 C. R. Matos-Pérez, J. D. White and J. J. Wilker, *J. Am. Chem. Soc.*, 2012, **134**, 9498–9505.
20 L. Li, B. Yan, J. Yang, L. Chen and H. Zeng, *Adv. Mater.*, 2015, **27**, 1294–1299.
21 S. Seo, S. Das, P. J. Zalicki, R. Mirshafian, C. D. Eisenbach, J. N. Israelachvili, J. H. Waite and B. K. Ahn, *J. Am. Chem. Soc.*, 2015, **137**, 9214–9217.
22 M. R. Chapman, L. S. Robinson, J. S. Pinkner, R. Roth, J. Heuser, M. Hammar, S. Normark and S. J. Hultgren, *Science*, 2002, **295**, 851–855.
23 Y. Zhang, L. Tao, S. Li and Y. Wei, *Biomacromolecules*, 2011, **12**, 2894–2901.
24 J. Kang, V. K. Sangwan, J. D. Wood and M. C. Hersam, *Acc. Chem. Res.*, 2017, **50**, 943–951.
25 L. Xing, Q. Li, G. Zhang, X. Zhang, F. Liu, L. Liu, Y. Huang and Q. Wang, *Adv. Funct. Mater.*, 2016, **26**, 3524–3531.
26 Y. Chung, Y. Ahn, M. Christwardana, H. Kim and Y. Kwon, *Nanoscale*, 2016, **8**, 9201–9210.
27 W. Chen, T. Lei, T. Qian, W. Lv, W. He, C. Wu, X. Liu, J. Liu, B. Chen, C. Yan and J. Xiong, *Adv. Energy Mater.*, 2018, **8**, 1702889.
28 A. Li, Y. Mu, W. Jiang and X. Wan, *Chem. Commun.*, 2015, **51**, 9117–9120.
29 D. Hafner, L. Ziegler, M. Ichwan, T. Zhang, M. Schneider, M. Schiffmann, C. Thomas, K. Hinrichs, R. Jordan and I. Amin, *Adv. Mater.*, 2016, **28**, 1489–1494.
30 K. Zhan, C. Kim, K. Sung, H. Ejima and N. Yoshie, *Biomacromolecules*, 2017, **18**, 2959–2966.
31 A. H. Hofman, I. A. van Hees, J. Yang and M. Kamperman, *Adv. Mater.*, 2018, **30**, 1704640.
32 Q. Jiang and H. M. Lu, *Surf. Sci. Rep.*, 2008, 427–464.
33 M. Kim and H. Chung, *Polym. Chem.*, 2017, 6300–6308.
34 H. Kim, H. Mohapatra and S. T. Phillips, *Angew. Chem.*, 2015, **127**, 13255–13259.
35 J. Ping, F. Gao, J. L. Chen, R. D. Webster and T. W. J. Steele, *Nat. Commun.*, 2015, **6**, 8050.
36 D. Lu, H. Wang, T. Li, Y. Li, X. Wang, P. Niu, H. Guo, S. Sun, X. Wang, X. Guan, H. Ma and Z. Lei, *Chem. Mater.*, 2017, **29**, 5493–5503.
37 J. Liu and O. A. Scherman, *Adv. Funct. Mater.*, 2018, **28**, 1800848.
38 Q. Xiao, W. Han, R. Yang, Y. You, R. Wei and X. Liu, *Polym. Composite.*, 2018, **39**, 1598–1605.
39 X. Zhang, *Analysis and test technology of adhesive*, Chemical Industry Press, Beijing, 2004.
40 X. Yin, J. Chen, W. Yuan, Q. Lin, L. Ji and F. Liu, *Polym. Bull.*, 2012, **68**, 1215–1226.
41 F. Sayilkan, M. Asiltürk, N. Kiraz, E. Burunkaya, E. G. Arpac and H. Sayilkana, *J. Hazard. Mater.*, 2009, 1309–1316.